DASPy: A Python Toolbox for DAS Seismology

Minzhe Hu[1] and Zefeng Li[1, 2*]

1. Laboratory of Seismology and Physics of Earth's Interior, School of Earth and Space Sciences, University of Science and Technology of China, Hefei, China

2. Mengcheng National Geophysical Observatory, University of Science and Technology of China, Mengcheng, China

Corresponding author: Zefeng Li (zefengli@ustc.edu.cn)

Manuscript submitted to *Seismological Research Letters*

June 12th, 2024

Abstract

Distributed acoustic sensing (DAS) has emerged as a novel technology in geophysics, owing to its high sensing density, cost-effectiveness, and adaptability to extreme environments. Nonetheless, DAS differs from traditional seismic acquisition technologies in many aspects: big data volume, equidistant sensing, measurement of axial strain (strain rate), and noise characteristics. These differences make DAS data processing challenging for new hands. To lower the bar of DAS data processing, we develop an open-source Python toolbox called DASPy, which encompasses classic seismic data processing techniques, including preprocessing, filter, spectrum analysis, and visualization, and specialized algorithms for DAS applications, including denoising, waveform decomposition, channel attribute analysis, and strain-velocity conversion. Using openly available DAS data as examples, this paper makes an overview and tutorial on the eight modules in DASPy to illustrate the algorithms and practical applications. We anticipate DASPy to provide convenience for researchers unfamiliar with DAS data and help facilitate the rapid growth of DAS seismology.

1 Introduction

Distributed acoustic sensing (DAS) is an emerging vibration monitoring technology increasingly utilized in geophysics. It converts fiber optic cables into an ultradense seismic array with meter-scale spacing and a frequency range of 0.01 Hz to 100 kHz. DAS recovers axial strain or strain rate along the fiber-optic cable by measuring the subtle optical phase shift of backscattered light within the fiber (Lindsey & Martin, 2021; Zhan, 2019). Over recent years, it has been demonstrated useful in many seismological applications such as earthquake monitoring (Z. Li et al., 2021; Z. Li & Zhan, 2018; Lindsey et al., 2017; Nayak et al., 2021; Zeng et al., 2022), source properties (Chen, 2023; J. Li, Kim, et al., 2023; J. Li, Zhu, et al., 2023), subsurface imaging (Ajo-Franklin et al., 2019; Cheng et al., 2021; Dou et al., 2017; Luo et al., 2021; Nayak & Ajo-Franklin, 2021; Yang, Atterholt, et al., 2022), fault zone structures (Atterholt, Zhan, & Yang, 2022; Jousset et al., 2018; Lindsey et al., 2019; Yang, Zhan, et al., 2022) and urban seismology (Lindsey, Yuan, et al., 2020; X. Wang et al., 2021; Zhu et al., 2021). It has also been applied in volcanology (Jousset et al., 2022; Nishimura et al., 2021), oceanography (Lin et al., 2024; Sladen et al., 2019; Williams et al., 2019, 2022; Xiao et al., 2022), glaciology (Hudson et al., 2021; Walter et al., 2020), marine biology (Bouffaut et al., 2022; Landrø et al., 2022; Rørstadbotnen et al., 2023; Wilcock et al., 2023), and meteorology (Hong et al., 2024; Zhu & Stensrud, 2019).

DAS is distinct from conventional seismometers in several key aspects, including the voluminous data, the regular spacing of sensors, and the uniaxial measurement of strain or strain rate (Z. Li, 2021). The noise composition of DAS tends to be more complex due to its different self-noise, common-mode noise, and traffic noise for often along-road fibers (Bakku, 2015; Costa et al., 2019; Lindsey, Rademacher, et al., 2020; Zhirnov et al., 2019). These differences often require different processing techniques from those for conventional seismometers, making it challenging for researchers newly using DAS data. Due to the similarities in the regular spacing characteristics of DAS and seismic exploration, it is feasible to process DAS data using seismic data processing software suitable for exploration data, such as SU (Cohen & Stockwell, 2008) and Madagascar (http://www.reproducibility.org). Nonetheless, the requirements for DAS channel analysis and data unit conversion cannot be fulfilled through this way. Inspired by the success of ObsPy for conventional seismic data processing (Beyreuther et al., 2010), we believe that a new Python processing package specifically designed for DAS data could facilitate the development of DAS seismology. Another ongoing development worth noting is DASCore, which realized reading and writing, visualization, and basic processing of DAS data in various file formats (Chambers et al., 2024). Despite this, we still desire to provide more diverse data processing functions and dedicated tools.

In this paper, we design an open-source Python package named DASPy for DAS data processing. This package comprises two primary components: a set of basic tools including modules for preprocessing, filtering, frequency attributes and visualization, and another set of advanced tools including modules for channel analysis, waveform decomposition, denoising and strain-velocity conversion (Fig. 1). As follows, we showcase the key functionalities using various publicly available datasets (Fig. 2) and ensure that the experiments can be easily replicated by readers.

2 Basic Tools

2.1 Classic processing techniques

Typical seismic data processing includes filtering, frequency attribute analysis and certain preprocessing methods. We wrap these techniques for 2D DAS data, eliminating the need for iterating over channels. For example, the Python code below bandpass filters the data from the RAPID dataset (Wilcock & Ocean Observatories Initiative., 2023; http://piweb.ooirsn.uw.edu/das/; Figure 2a) between 15 and 27 Hz and yields a spectrogram averaged over 100 channels and a frequency-wavenumber (FK) spectrum (Figure 3). This dataset was collected offshore central Oregon and recorded various signals including fin whale calls, northeast Pacific blue whale A and B calls, and ship noises (Wilcock et al., 2023).

```
>>> from daspy.basic_tools.filter import bandpass
>>> from daspy.basic_tools.freqattributes import spectrogram, fk_transform
>>>
>>> data_filtered = bandpass(data, fs, 15, 27, detrend=True, taper=0.04)
>>> spec, f1, t = spectrogram(data[4880-50:4880+50], fs=fs, nperseg=256, noverlap=246,
                               nfft=1024, detrend=True)
>>> fk, f2, k = fk_transform(data, dx, fs)
```

2.2 Visualization

The function, `plot`, can be used to visualize 2D DAS data. It offers a number of optional parameters to accommodate the users' requirements for plotting a variety of data types, such as waveforms, spectra, spectrograms, and FK spectra. Below is the Python code for visualizing the data in the previous example: unfiltered and filtered data, the spectrogram and the FK spectrum (Figure 3). The bandpass filtered waveform reveals high-frequency fin whale calls, with amplitudes approximately four to five orders of magnitude lower than the ocean wave signals (Figure 3b). The spectrogram demonstrates the sequential production of high- and low-frequency calls by the fin whale (Figure 3c). The FK spectrum reveals an apparent velocity of this acoustic signal exceeding 1400 m/s along the axial direction of the optical cable (Figure 3d).

```
>>> from daspy.basic_tools.visualization import plot
>>>
>>> fig, ax = plt.subplots(4, 1, figsize=(7,8))
>>> plot(data, dx=dx, fs=fs, ax=ax[0], transpose=True, x0=xmin*dx, xlabel=False,
          colorbar_label='Strain')
>>> plot(data_filtered, dx=dx, fs=fs, ax=ax[1], transpose=True, x0=xmin*dx,
          xlabel=False, colorbar_label='Strain')
>>> plot(Zxx, fs=fs, obj='spectrogram', ax=ax[2], f=f1, t=t, vmin=2e-8, vmax=3e-6,
        ylim=[0, 40])
>>> plot(fk, obj='fk', ax=ax[3], f=f2, k=k, xlim=[-0.025, 0.025], ylim=[0, 40],
        vmin=0.05, vmax=0.2)
>>> plt.tight_layout(pad=0.5)
>>> plt.savefig('figure3.pdf', dpi=1200)
```

3 Advanced Tools

3.1 Channel analysis

DAS channels have equidistant spacing but the location of each channel is often unknown and requires tap tests. Besides, the linearity and ground coupling of the fibers often need to be taken care of. We develop three functions for channel location and quality analysis: channel location interpolation, turning point detection, and low-quality channel checking.

Channel location interpolation for DAS is calculated using two types of inputs: points with known channel numbers, and optional fiber spatial track points without channel numbers. Points with known channel numbers are typically acquired through tap tests and are often sparse. The spatial fiber track points are used to constrain the array geometry. They are optional but dense track points are particularly useful for accurate location interpolation. Fig. 2a shows examples of the two DAS arrays of the RAPID dataset (Wilcock & Ocean Observatories Initiative., 2023). In DASPy, we implemented the interpolation method used by the RAPID team, in which interpolation is performed after the coordinates are projected to the Universal Transverse Mercator (UTM) coordinate system.

The turning point detection function determines the points where the fiber strike varies noticeably based on the given channel coordinates or based on waveform coherency across neighboring channels. The application of the coordinate-based detection function to Brady's geothermal field DAS array (University of Wisconsin, 2016a; https://gdr.openei.org/submissions/829; Fig. 2c) produces results consistent with those of Piana Agostinetti et al. (2022). As across-channel waveform coherency is not only affected by the fiber strike angle, but also controlled by other factors including the quality of the backscattered light, coupling conditions and small-scale scatterers at different locations, its results could be less stable than those of coordinate-based computations assuming the coordinates are accurate. However, when the coordinates are unavailable or inaccurate, inference from across-channel waveform coherency could be a suitable alternative.

The channel quality checking function detects segments with obvious poor coupling (e.g., zip-tied loops of telecommunication cables) by identifying outliers of waveform energy along the fiber. It fits the waveform energy (the square of the amplitudes) variations with channels by a high-order polynomial and removes the fitted polynomial from the data. A threshold of four times of standard deviation below the median is set to identify the outliers. We assume that poor coupling tends to be spatially continuous. Hence, isolated normal values among a group of outliers would be identified as bad channels and vice versa. Using this function, we assess the channel quality of Ridgecrest DAS (Fig. 2d) with 15 seconds of traffic noise (Atterholt, 2021; https://data.caltech.edu/records/1955, Fig. 4). Our waveform-based detection results are generally consistent with the hand-picked results of Atterholt, Zhan, Shen, et al.

(2022) (Fig. 4b-f), except for the initial segment which was identified from a priori knowledge during field installation. It is noteworthy that the spikes (Fig. 4a) do not significantly influence the low-quality channel detection because we use a robust fit for the waveform energy (abnormal points are excluded from fitting).

3.2 Data denoising

As aforementioned, DAS data are often mixed with complex types of noise. DASPy integrates functions for the removal of typical noise types, including spike noise (Bakku, 2015), common-mode noise (Lindsey, Rademacher, et al., 2020), stochastic noise (Costa et al., 2019), and coherent noise. DASPy constructs a denoising module that incorporates three methods that take advantage of different noise properties.

Spikes are unusually large amplitudes (Fig. 5a) and could be caused by laser frequency drift or laser noise (Zhirnov et al., 2019). The spike removal function first applies the across-channel median filter and then the across-time median filter to generate a median map from the absolute amplitudes. Points with amplitudes exceeding a predefined threshold of the median map are identified as spikes. All spikes are subsequently substituted with interpolated values from adjacent channels. The spike removal function is validated using an earthquake waveform recorded by the Stanford-1 DAS array (Fig. 2b and Fig. 5a-b; Biondi et al., 2017; Martin et al., 2017).

Common-mode noise, also known as in-phase noise is generated by vibrations of the optoelectronic system and arises on all channels simultaneously (Fig. 5d). DASPy employs spatial averaging of waveforms to obtain common mode noise. Subsequently, we compute the correlation coefficient with the channel record and the common-mode noise, multiply the common-mode noise by the coefficient, and subtract it from the channel record. We evaluate the common-mode noise removal algorithm using a segment of offshore channels of the RAPID dataset (Wilcock & Ocean Observatories Initiative, 2023; Fig. 2a). The processing effectively mitigates the common-mode noise (Fig. 5d-e).

The inherent stochastic noise in DAS data is primarily caused by instrumental deficiencies such as sampling error and phase noise (Costa et al., 2019). The fast discrete curvelet transform (FDCT) (E. Candès et al., 2006; E. J. Candès & Donoho, 2004) is used to obtain an effective non-adaptive sparse representation of the regular-spaced DAS seismic data and remove stochastic noise (Atterholt, Zhan, Shen, et al., 2022). The basis functions of curvelet transform are defined as polar wedges in the FK domain and represent the object position, scale, and angle. The curvelet denoising function uses a silent DAS recording to estimate stochastic noise. After FDCT, the amplitude of the curvelet coefficients is used as an empirical threshold. By default, DASPy employs a soft threshold to remove stochastic noise in the curvelet domain. We apply curvelet denoising to the spike-removed waveform of Stanford-1 DAS (Biondi et al., 2017; Martin et al., 2017; Fig. 2b and Fig. 5b), resulting in a notable reduction in stochastic noise before the arrival of P waves (Fig. 5c).

Coherent noise can be defined as any coherent signal that are not of interest. For example, for studies on an earthquake, a traffic signal is coherent noise; for studies on traffic footprints, an earthquake signal is coherent noise. Coherent noise can be removed by applying velocity screening in either the curvelet transform or the FK transform. In this case, coherent noise removal is treated as wavefield decomposition based on apparent velocity, which will be elaborated upon in the subsequent section.

3.3 Wavefield decomposition

Image processing techniques, such as the 2D Fast Fourier Transform (e.g., FK transform in DAS data processing) and FDCT, have been widely used in the decomposition of 2D DAS wavefields, such as the separation of seismic signals and traffic noise and the separation of direct seismic waves and locally scattered seismic waves (Atterholt, Zhan, Shen, et al., 2022; Williams et al., 2022). DASPy integrates the FK filtering and curvelet windowing techniques in the decomposition module. Note that FK filtering often causes various artifacts, particularly edge artifacts caused by discontinuities at the waveform’s edge, and star-like artifacts originating from discontinuities in the FK domain. To minimize these artifacts, DASPy employs cosine tapers (e.g. Tukey window) on the waveforms, as well as the filtering window in the FK domain.

Both wavefield decomposition techniques are evaluated on stripping traffic noise from seismic waveform from the Ridgecrest DAS array (Z. Li et al., 2021; Fig. 2d). The results show that both techniques effectively enhance the signal-to-noise ratio (Fig. 6). In the curvelet transform, the finest objects can be represented by wavelets (more efficient) or curvelets (more precise). When utilizing curvelets for the finest representation, there is no significant difference between the results of FK filtering and curvelet windowing techniques integrated in DASPy (Fig. 6b-e).

3.4 Conversion to ground motions

DAS measures strain or strain rate, in contrast to ground-motion velocity and displacement used in typical seismology studies. Starin and strain rate can be converted to particle velocity and acceleration by multiplying apparent phase velocity. The difficulty of such conversion lies in the accurate estimation of apparent phase velocity of every wiggle. DASPy integrates three methodologies for converting strain/strain rate into ground-motion velocity: FK rescaling (Lindsey, Rademacher, et al., 2020), curvelet transform (Yang, Atterholt, et al., 2022), and time-domain slowness determination (Lior et al., 2021). The FK rescaling method is implemented by multiplying each point in the FK domain by its corresponding apparent velocity (slop in the FK domain). Similarly, the basis functions of the curvelet transform, which are defined in the FK domain, also correspond to varying velocity ranges. The curvelet transform conversion method multiplies each curvelet coefficient by the median velocity of its basis function. The coefficients of the largest scale basis functions, which represents waves with all velocity ($-\infty$ to $+\infty$), is set to zero. The time-domain slowness determination method obtains the apparent velocity at each time step by searching for the maximal semblance.

These three methods are tested using an M_L 4.3 earthquake recorded by a co-located DAS and seismometer array in the Brady Hot Springs (University of Wisconsin, 2016b; University of Wisconsin, 2016c; https://gdr.openei.org/submissions/848; https://gdr.openei.org/submissions/846; Fig. 3c), following H. F. Wang et al. (2018). We define a nodal geophone and a DAS channel whose distance is less than 5 m as a geophone-channel pair. Among 238 geophones and 8,621 DAS channels, we match a total of 344 geophone-channel pairs. For each geophone-channel pair, we find the corresponding linear DAS segment (Fig. 2c) and rotate the three-component geophone recording to the axial fiber direction. The original DAS strain rate recordings are integrated to strain in the time domain, and converted to velocity using FK rescaling, curvelet transform and time-domain slowness determination methods respectively (Fig. 7). We correct the DAS data timing (-1.048 s) using the GPS timing of nodal seismometers, and cross-correlate the waveforms of each geophone-channel pair with time shift less than ±0.01 seconds. All waveforms are bandpass filtered to 1-5 Hz.

We evaluate the cross-correlation coefficient between the converted DAS velocity and the rotated geophone velocity. For all 344 geophone-channel pairs, 104, 71 and 0 pairs obtain cross-correlation coefficients greater than 0.7 after FK rescaling, curvelet transformation and time-domain slowness determination, respectively. For this particular case, the curvelet transform and the time-domain slowness determination have limitations. Most linear segments consist of about 100 channels, which is not quite enough for curvelet transform at larger scales. The largest scale curvelet coefficients, which are set to zero, miss more details, resulting in smaller amplitudes of the converted waveforms (Fig. 7). As for time-domain slowness determination methods, the assumption of monochromatic wavefields makes it difficult to recover the complex shallow surface scattered waves and earthquake coda waves.

4 Discussion and conclusions

DASPy aims to offer a user-friendly, integrated Python toolkit that facilitates the analysis and processing of DAS data. Overall, the toolkit includes “basic tools” of preprocessing, filtering, spectrum analysis, and visualization techniques and “advanced tools” of channel attribute analysis, noise removal, wavefield decomposition, and strain-velocity conversion.

DASPy operates in the form of functions, which are designed to accommodate as many optional parameters as possible, and with sensible default values. All functions within DASPy are implemented as methods of the "daspy.DASdata" class. This approach is advantageous in that data attributes are stored within the class and avoid the need for manual entry. Calling functions and using methods of “daspy.Section” class are functionally equivalent, providing flexibility to suit users’ needs. Through DASPy's built-in read and write functions and object-oriented programming, DASPy can be easily incorporated into the data up- and down-stream. The following is an example code snippet for data preprocessing, specifically for a phase picking task:

```
>>> from daspy import read
>>>
>>> sec = (
>>>     read('raw_data.h5')
>>>     .spike_removal()
>>>     .downsampling(xint=10, tint=10)
>>>     .fk_filter(fmin=1, fmax=15, vmin=2000)
>>> )
>>> sec.plot()
>>> sec.save('preprocessed_data.h5')
```

The code reads in DAS data into an instance of “daspy.Section”, removes spike noise, performs a tenfold downsampling in both distance dimension (stacking every 10 channels into one) and time dimension (after an automatic lowpass filter), and separates signal with frequency of 1-15Hz and apparent velocity less than 2000 m/s using FK filter. The processed waveform is then visualized and saved for use by down-stream phase picking tools. DASPy is capable of both reading and writing various DAS file formats, encompassing .h5, .segy/.sgy, .tdms and .pkl (used for storing “daspy.Section” instances). Moreover, DASPy enables the conversion of dascore’s “Patch” instances

(Chambers et al., 2024) into “daspy.Section” instances, facilitated by the class method “Section.from_dascore_patch”. DASPy also supports the reading of metadata in DAS-RCN format and the generation of new “daspy.Section” instances, inheriting attributes from the source file. (Lai et al., 2024).

DASPy is currently programmed in pure Python for ease of use and modification but in some cases computational efficiency is compromised. Consequently, processing continuous data with a large number of channels and/or a high sampling rate could take a long time. As an example, downsampling a 30-second waveform recorded at 1000 Hz by a 10,000-channel DAS array takes 12.08 seconds. Therefore, we suggest that users consider implementing CPU parallelization when undertaking large tasks. Future development of DASPy could include exploring the potential of shared libraries to replace computationally intensive functions.

Finally, we welcome users to contribute to the improvement and expansion of the DASPy project by developing new functions and/or modules (such as earthquake monitoring, ambient noise imaging, and traffic detection algorithms) upon the foundation of existing functionalities. Users are recommended to fork the DASPy repository on Github (https://github.com/HMZ-03/DASPy/) and submit their modifications and additions through pull requests.

Data and Resources

The RAPID dataset is openly available at http://piweb.ooirsn.uw.edu/das/. The traffic signals recorded by the Ridgecrest DAS can be downloaded from https://data.caltech.edu/records/31emd-wmv98. The Stanford DAS-1 dataset from PubDAS is accessible via the link https://app.globus.org/file-manager?origin_id=706e304c-5def-11ec-9b5c-f9dfb1abb183&origin_path=%2F. The earthquake waveforms recorded by Brady's Geothermal Field DAS and seismometer array are available at https://gdr.openei.org/submissions/848 and https://gdr.openei.org/submissions/846. The DASPy python package is open source and available at https://github.com/HMZ-03/DASPy/. All websites were last accessed in March 2024.

Acknowledgements

This research was supported by the National Key R&D Program of China (No. 2022YFC3005602).

Declaration of Competing Interests

The authors acknowledge there are no conflicts of interest recorded.

References

Ajo-Franklin, J. B., Dou, S., Lindsey, N. J., Monga, I., Tracy, C., Robertson, M., et al. (2019). Distributed Acoustic Sensing Using Dark Fiber for Near-Surface Characterization and Broadband Seismic Event Detection. *Scientific Reports*, *9*(1), 1–14. https://doi.org/10.1038/s41598-018-36675-8

Atterholt, J. (2021). Earthquake Waveforms from Curvelet-denoising Paper (Data Supplement) (1.0) [Data set]. CaltechDATA. https://doi.org/10.22002/D1.1955

Atterholt, J., Zhan, Z., Shen, Z., & Li, Z. (2022). A unified wavefield-partitioning approach for distributed acoustic sensing. *Geophysical Journal International*, *228*(2), 1410–1418. https://doi.org/10.1093/gji/ggab407

Atterholt, J., Zhan, Z., & Yang, Y. (2022). Fault zone imaging with distributed acoustic sensing: body-to-surface wave scattering. *Journal of Geophysical Research: Solid Earth*, *127*(6), 1–17. https://doi.org/10.1029/2022jb024329

Bakku, S. K. (2015). Fracture Characterization from Seismic Measurements in a Borehole. *PhD Thesis*.

Beyreuther, M., Barsch, R., Krischer, L., Megies, T., Behr, Y., & Wassermann, J. (2010). ObsPy: A python toolbox for seismology. *Seismological Research Letters*, *81*(3), 530–533. https://doi.org/10.1785/gssrl.81.3.530

Biondi, B., Martin, E., Cole, S., Karrenbach, M., & Lindsey, N. (2017). Earthquakes analysis using data recorded by the Stanford DAS array. In *SEG Technical*

Program Expanded Abstracts 2017 (pp. 2752–2756). https://doi.org/10.1190/segam2017-17745041.1

Bouffaut, L., Taweesintananon, K., Kriesell, H. J., Rørstadbotnen, R. A., Potter, J. R., Landrø, M., et al. (2022). Eavesdropping at the Speed of Light: Distributed Acoustic Sensing of Baleen Whales in the Arctic. *Frontiers in Marine Science*, *9*(July), 1–13. https://doi.org/10.3389/fmars.2022.901348

Brady's Geothermal Field DAS and DTS Surface and Borehole Array Metadata [Data set]. (2016). University of Wisconsin. https://doi.org/10.15121/1261907

Brady's Geothermal Field DAS Earthquake Data [Data set]. (2016). University of Wisconsin. https://doi.org/10.15121/1334285

Brady's Geothermal Field Nodal Seismometer Earthquake Data [Data set]. (2016). University of Wisconsin. https://doi.org/10.15121/1334284

Candès, E., Demanet, L., Donoho, D., & Ying, L. (2006). Fast discrete curvelet transforms. *Multiscale Modeling and Simulation*, *5*(3), 861–899. https://doi.org/10.1137/05064182X

Candès, E. J., & Donoho, D. L. (2004). New tight frames of curvelets and optimal representations of objects with piecewise C2 singularities. *Communications on Pure and Applied Mathematics*, *57*(2), 0219–0266. https://doi.org/10.1002/cpa.10116

Chambers, D., Jin, G., Tourei, A., Hafiz Saeed Issah, A., Lellouch, A., Martin, E. R., et al. (2024). DASCore: a Python Library for Distributed Fiber Optic Sensing.

Chen, X. (2023). Source parameter analysis using distributed acoustic sensing – an example with the PoroTomo array. *Geophysical Journal International*, 2207–2213.

Cheng, F., Chi, B., Lindsey, N. J., Dawe, T. C., & Ajo-Franklin, J. B. (2021). Utilizing distributed acoustic sensing and ocean bottom fiber optic cables for submarine structural characterization. *Scientific Reports*, *11*(1), 1–14. https://doi.org/10.1038/s41598-021-84845-y

Cohen, J. K., & Stockwell, J. W. (2008). CWP/SU: Seismic Un*x: an open source software package for seismic research and processing. *Center for Wave Phenomena, Colorado School of Mines*, 40.

Costa, L., Martins, H. F., Martín-López, S., Fernández-Ruiz, M. R., & González-Herráez, M. (2019). Fully Distributed Optical Fiber Strain Sensor With 10−12 ϵ/√Hz Sensitivity. *Journal of Lightwave Technology*, *37*(18), 4487–4495. https://doi.org/10.1109/JLT.2019.2904560

Dou, S., Lindsey, N., Wagner, A. M., Daley, T. M., Freifeld, B., Robertson, M., et al. (2017). Distributed Acoustic Sensing for Seismic Monitoring of the Near Surface: A Traffic-Noise Interferometry Case Study. *Scientific Reports*, *7*(1), 1–12. https://doi.org/10.1038/s41598-017-11986-4

Hong, H., Wang, B., Lu, G., Li, X., Ge, Q., Xie, A., et al. (2024). Tracking Lightning Through 3D Thunder Source Location With Distributed Acoustic Sensing.

Journal of Geophysical Research: Atmospheres, *129*(4), 1–13. https://doi.org/10.1029/2023JD038882

Hudson, T. S., Baird, A. F., Kendall, J. M., Kufner, S. K., Brisbourne, A. M., Smith, A. M., et al. (2021). Distributed Acoustic Sensing (DAS) for Natural Microseismicity Studies: A Case Study From Antarctica. *Journal of Geophysical Research: Solid Earth*, *126*(7), 1–19. https://doi.org/10.1029/2020JB021493

Jousset, P., Currenti, G., Schwarz, B., Chalari, A., Tilmann, F., Reinsch, T., et al. (2018). Dynamic strain determination using fibre-optic cables allows imaging of seismological and structural features. *Nature Communications*, *13*(1). https://doi.org/10.1038/s41467-022-29184-w

Jousset, P., Currenti, G., Schwarz, B., Chalari, A., Tilmann, F., Zuccarello, L., et al. (2022). Fibre optic distributed acoustic sensing of volcanic events. *Nature Communications*. https://doi.org/10.1038/s41467-022-29184-w

Lai, V. H., Hodgkinson, K. M., Porritt, R. W., & Mellors, R. (2024). Toward a Metadata Standard for Distributed Acoustic Sensing (DAS) Data Collection. *Seismological Research Letters*, *95*(3), 1986–1999. https://doi.org/10.1785/0220230325

Landrø, M., Bouffaut, L., Kriesell, H. J., Potter, J. R., Rørstadbotnen, R. A., Taweesintananon, K., et al. (2022). Sensing whales, storms, ships and earthquakes using an Arctic fibre optic cable. *Scientific Reports*, *12*(1), 1–10. https://doi.org/10.1038/s41598-022-23606-x

Li, J., Zhu, W., Biondi, E., & Zhan, Z. (2023). Earthquake focal mechanisms with distributed acoustic sensing. *Nature Communications*, *14*(1), 4181. https://doi.org/10.1038/s41467-023-39639-3

Li, J., Kim, T., Lapusta, N., Biondi, E., & Zhan, Z. (2023). The break of earthquake asperities imaged by distributed acoustic sensing. *Nature*, *620*(October 2022). https://doi.org/10.1038/s41586-023-06227-w

Li, Z. (2021). Recent advances in earthquake monitoring i: Ongoing revolution of seismic instrumentation. *Earthquake Science*, *34*(2), 177–188. https://doi.org/10.29382/eqs-2021-0011

Li, Z., & Zhan, Z. (2018). Pushing the limit of earthquake detection with distributed acoustic sensing and template matching: A case study at the Brady geothermal field. *Geophysical Journal International*, *215*(3), 1583–1593. https://doi.org/10.1093/gji/ggy359

Li, Z., Shen, Z., Yang, Y., Williams, E., Wang, X., & Zhan, Z. (2021). Rapid Response to the 2019 Ridgecrest Earthquake With Distributed Acoustic Sensing. *AGU Advances*, *2*(2). https://doi.org/10.1029/2021av000395

Lin, J., Fang, S., He, R., Tang, Q., Qu, F., Wang, B., & Xu, W. (2024). Monitoring ocean currents during the passage of Typhoon Muifa using optical-fiber distributed acoustic sensing. *Nature Communications*, *15*(1). https://doi.org/10.1038/s41467-024-45412-x

Lindsey, N. J., & Martin, E. R. (2021). Fiber-Optic Seismology. *Annual Review of Earth and Planetary Sciences*, 309–338.

Lindsey, N. J., Martin, E. R., Dreger, D. S., Freifeld, B., Cole, S., James, S. R., et al. (2017). Fiber-Optic Network Observations of Earthquake Wavefields. *Geophysical Research Letters*, *44*(23), 11,792-11,799. https://doi.org/10.1002/2017GL075722

Lindsey, N. J., Craig Dawe, T., & Ajo-Franklin, J. B. (2019). Illuminating seafloor faults and ocean dynamics with dark fiber distributed acoustic sensing. *Science*, *366*(6469), 1103–1107. https://doi.org/10.1126/science.aay5881

Lindsey, N. J., Yuan, S., Lellouch, A., Gualtieri, L., Lecocq, T., & Biondi, B. (2020). City-Scale Dark Fiber DAS Measurements of Infrastructure Use During the COVID-19 Pandemic. *Geophysical Research Letters*, *47*(16), 1–8. https://doi.org/10.1029/2020GL089931

Lindsey, N. J., Rademacher, H., & Ajo-Franklin, J. B. (2020). On the Broadband Instrument Response of Fiber-Optic DAS Arrays. *Journal of Geophysical Research: Solid Earth*, *125*(2), 1–16. https://doi.org/10.1029/2019JB018145

Lior, I., Sladen, A., Mercerat, D., Ampuero, J. P., Rivet, D., & Sambolian, S. (2021). Strain to ground motion conversion of distributed acoustic sensing data for earthquake magnitude and stress drop determination. *Solid Earth*, *12*(6), 1421–1442. https://doi.org/10.5194/se-12-1421-2021

Luo, B., Trainor-Guitton, W., Bozdag, E., LaFlame, L., Cole, S., & Karrenbach, M. (2021). Horizontally orthogonal distributed acoustic sensing array for earthquake- And ambient-noise-based multichannel analysis of surface waves. *Geophysical Journal International*, *222*(3), 2147–2161. https://doi.org/10.1093/GJI/GGAA293

Martin, E., Castillo, C., Cole, S., Sawasdee, P., Yuan, S., Clapp, R., et al. (2017). Seismic monitoring leveraging existing telecom infrastructure at the SDASA: Active, passive, and ambient-noise analysis. *The Leading Edge*, *36*, 1025–1031. https://doi.org/10.1190/tle36121025.1

Nayak, A., & Ajo-Franklin, J. (2021). Measurement of surface-wave phase-velocity dispersion on mixed inertial seismometer – distributed acoustic sensing seismic noise cross-correlations. *Bulletin of the Seismological Society of America*, *111*(6), 3432–3450. https://doi.org/10.1785/0120210028

Nayak, A., Ajo-Franklin, J., & Team, the I. V. D. F. (2021). Distributed Acoustic Sensing Using Dark Fiber for Array Detection of Regional Earthquakes. *Seismological Research Letters*, *92*(4), 2441–2452. https://doi.org/10.1785/0220200416

Nishimura, T., Emoto, K., Nakahara, H., Miura, S., Yamamoto, M., Sugimura, S., et al. (2021). Source location of volcanic earthquakes and subsurface characterization using fiber-optic cable and distributed acoustic sensing system. *Scientific Reports*, *11*(1), 1–12. https://doi.org/10.1038/s41598-021-85621-8

Piana Agostinetti, N., Villa, A., & Saccorotti, G. (2022). Distributed acoustic sensing as a tool for subsurface mapping and seismic event monitoring: A proof of concept. *Solid Earth, 13*(2), 449–468. https://doi.org/10.5194/se-13-449-2022

Rørstadbotnen, R. A., Eidsvik, J., Bouffaut, L., Landrø, M., Potter, J., Taweesintananon, K., et al. (2023). Simultaneous tracking of multiple whales using two fiber-optic cables in the Arctic. *Frontiers in Marine Science*, *10*(April), 1–15. https://doi.org/10.3389/fmars.2023.1130898

Sladen, A., Rivet, D., Ampuero, J. P., De Barros, L., Hello, Y., Calbris, G., & Lamare, P. (2019). Distributed sensing of earthquakes and ocean-solid Earth interactions on seafloor telecom cables. *Nature Communications, 10*(1), 1–8. https://doi.org/10.1038/s41467-019-13793-z

Walter, F., Gräff, D., Lindner, F., Paitz, P., Köpfli, M., Chmiel, M., & Fichtner, A. (2020). Distributed acoustic sensing of microseismic sources and wave propagation in glaciated terrain. *Nature Communications, 11*(1). https://doi.org/10.1038/s41467-020-15824-6

Wang, H. F., Zeng, X., Miller, D. E., Fratta, D., Feigl, K. L., Thurber, C. H., & Mellors, R. J. (2018). Ground motion response to an ML 4.3 earthquake using co-located distributed acoustic sensing and seismometer arrays. *Geophysical Journal International, 213*(3), 2020–2036. https://doi.org/10.1093/GJI/GGY102

Wang, X., Zhan, Z., Williams, E. F., Herráez, M. G., Martins, H. F., & Karrenbach, M. (2021). Ground vibrations recorded by fiber-optic cables reveal traffic response to COVID-19 lockdown measures in Pasadena, California. *Communications Earth & Environment*, *2*(1), 1–9. https://doi.org/10.1038/s43247-021-00234-3

Wilcock, W. S. D., & Ocean Observatories Initiative. (2023). Rapid: A Community Test of Distributed Acoustic Sensing on the Ocean Observatories Initiative Regional Cabled Array [Data set]. Ocean Observatories Initiative. https://doi.org/doi.org/10.58046/5J60-FJ89

Wilcock, W. S. D., Abadi, S., & Lipovsky, B. P. (2023). Distributed acoustic sensing recordings of low-frequency whale calls and ship noise offshore Central Oregon. *JASA Express Letters*, *3*(2), 026002. https://doi.org/10.1121/10.0017104

Williams, E. F., Fernández-Ruiz, M. R., Magalhaes, R., Vanthillo, R., Zhan, Z., González-Herráez, M., & Martins, H. F. (2019). Distributed sensing of microseisms and teleseisms with submarine dark fibers. *Nature Communications*, *10*(1), 1–11. https://doi.org/10.1038/s41467-019-13262-7

Williams, E. F., Zhan, Z., Martins, H. F., Fernández-Ruiz, M. R., Martín-López, S., González-Herráez, M., & Callies, J. (2022). Surface Gravity Wave Interferometry and Ocean Current Monitoring With Ocean-Bottom DAS. *Journal of Geophysical Research: Oceans*, *127*(5), 1–27. https://doi.org/10.1029/2021JC018375

Xiao, H., Gaite, B., & Ruiz-barajas, S. (2022). Locating the precise sources of high-frequency microseisms using distributed acoustic sensing. *Geophysical Research Letters*, 0–31. https://doi.org/10.1029/2022GL099292

Yang, Y., Zhan, Z., Shen, Z., & Atterholt, J. (2022). Fault Zone Imaging With Distributed Acoustic Sensing: Surface-To-Surface Wave Scattering. *Journal of Geophysical Research: Solid Earth*, *127*(6). https://doi.org/10.1029/2022jb024329

Yang, Y., Atterholt, J. W., Shen, Z., Muir, J. B., Williams, E. F., & Zhan, Z. (2022). Sub-Kilometer Correlation Between Near-Surface Structure and Ground Motion Measured With Distributed Acoustic Sensing. *Geophysical Research Letters*, *49*(1). https://doi.org/10.1029/2021GL096503

Zeng, X., Bao, F., Thurber, C. H., Lin, R., Wang, S., Song, Z., & Han, L. (2022). Turning a Telecom Fiber-Optic Cable into an Ultradense Seismic Array for Rapid Postearthquake Response in an Urban Area. *Seismological Research Letters*, *93*(2 A), 853–865. https://doi.org/10.1785/0220210183

Zhan, Z. (2019). Distributed acoustic sensing turns fiber-optic cables into sensitive seismic antennas. *Seismological Research Letters*, *91*(1), 1–15. https://doi.org/10.1785/0220190112

Zhirnov, A., Stepanov, K., Chernutsky, A., Fedorov, A., Nesterov, E., Svelto, C., et al. (2019). Influence of laser frequency drift in phase-sensitive optical time-domain reflectometry. *Optics and Spectroscopy*, *127*. https://doi.org/10.1134/S0030400X1910031X

Zhu, T., & Stensrud, D. J. (2019). Characterizing Thunder-Induced Ground Motions Using Fiber-Optic Distributed Acoustic Sensing Array. *Journal of Geophysical Research: Atmospheres*, *124*(23), 12810–12823. https://doi.org/10.1029/2019JD031453

Zhu, T., Shen, J., & Martin, E. R. (2021). Sensing Earth and environment dynamics by telecommunication fiber-optic sensors: An urban experiment in Pennsylvania, USA. *Solid Earth*, *12*(1), 219–235. https://doi.org/10.5194/se-12-219-2021

Full mailing address for each author

Minzhe Hu: Laboratory of Seismology and Physics of Earth's Interior, School of Earth and Space Sciences, University of Science and Technology of China, No.96, JinZhai Road Baohe District, Hefei, Anhui, 230026, P.R.China.

Zefeng Li: Laboratory of Seismology and Physics of Earth's Interior, School of Earth and Space Sciences, University of Science and Technology of China, No.96, JinZhai Road Baohe District, Hefei, Anhui, 230026, P.R.China.

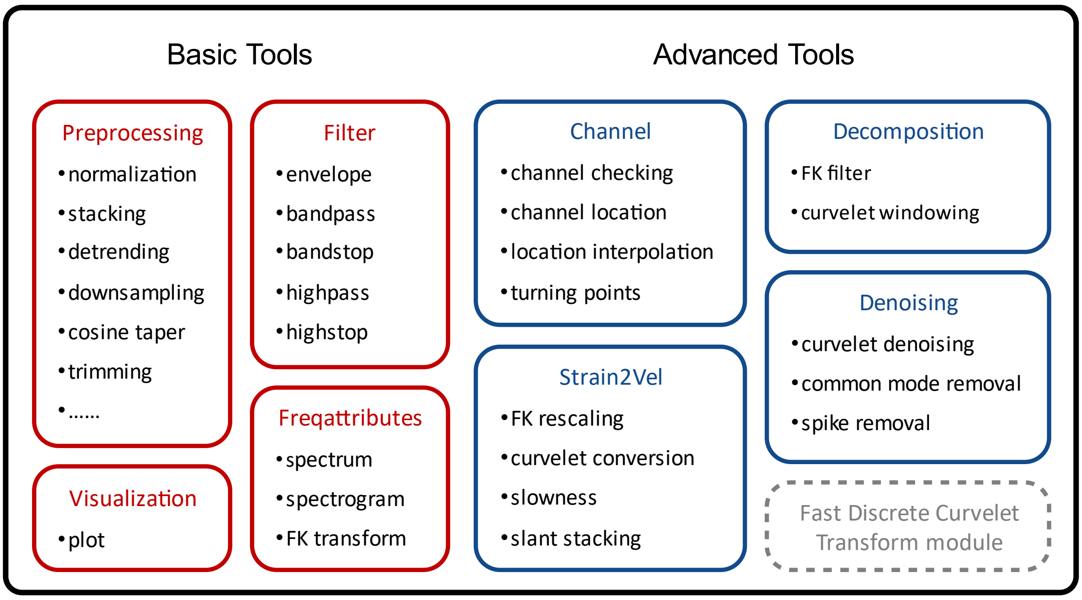

Figure 1. Main structure of DASPy toolbox. Each block indicates a module composed of multiple user-facing functions. The modules for basic tools are shown in red boxes, and modules for advanced tools are shown in blue boxes. The module within the gray dotted box is specifically built for discrete fast curvelet transforms.

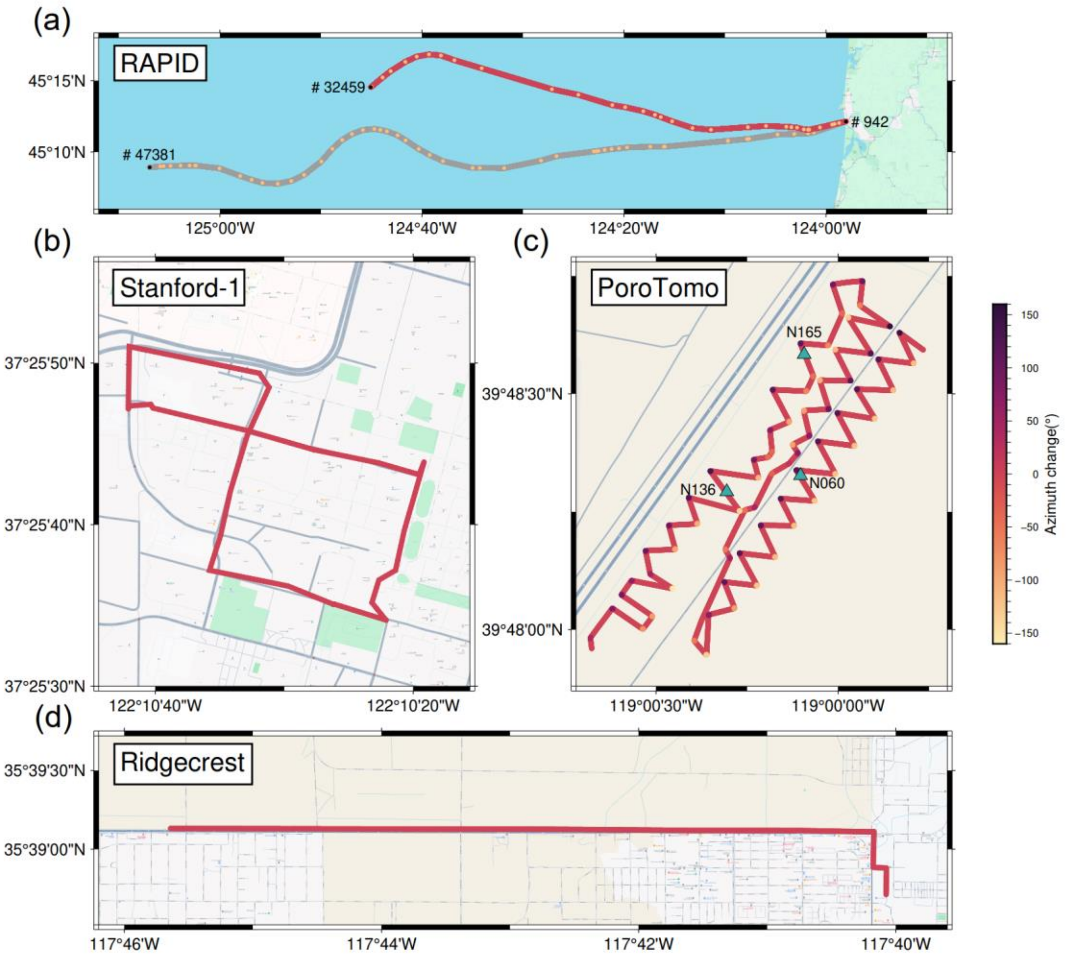

Figure 2. Geometry of DAS arrays whose data we used for testing. (a) RAPID DAS arrays that land at Pacific City, Oregon (Wilcock & Ocean Observatories Initiative., 2023). The red line indicates the array that we utilized for our test (referring to the north cable here), which is the same for (b) and (d). The grey line indicates the south cable, whose data are not used. The black dots represent three points along the cable with known coordinates and channel numbers, while the orange dots represent the those with known coordinates but unknown channel number. (b) Stanford campus array in California (Biondi et al., 2017; Martin et al., 2017). (c) Brady's geothermal field DAS array (University of Wisconsin, 2016b) and three co-located geophone stations

(University of Wisconsin, 2016c) in Nevada. The color of the DAS cable indicates the azimuth change of the cable before and after the corresponding channel. (d) DAS arrays started after the 2019 M_w7.1 Ridgecrest earthquake, California (Atterholt, Zhan, Shen, et al., 2022; Z. Li et al., 2021).

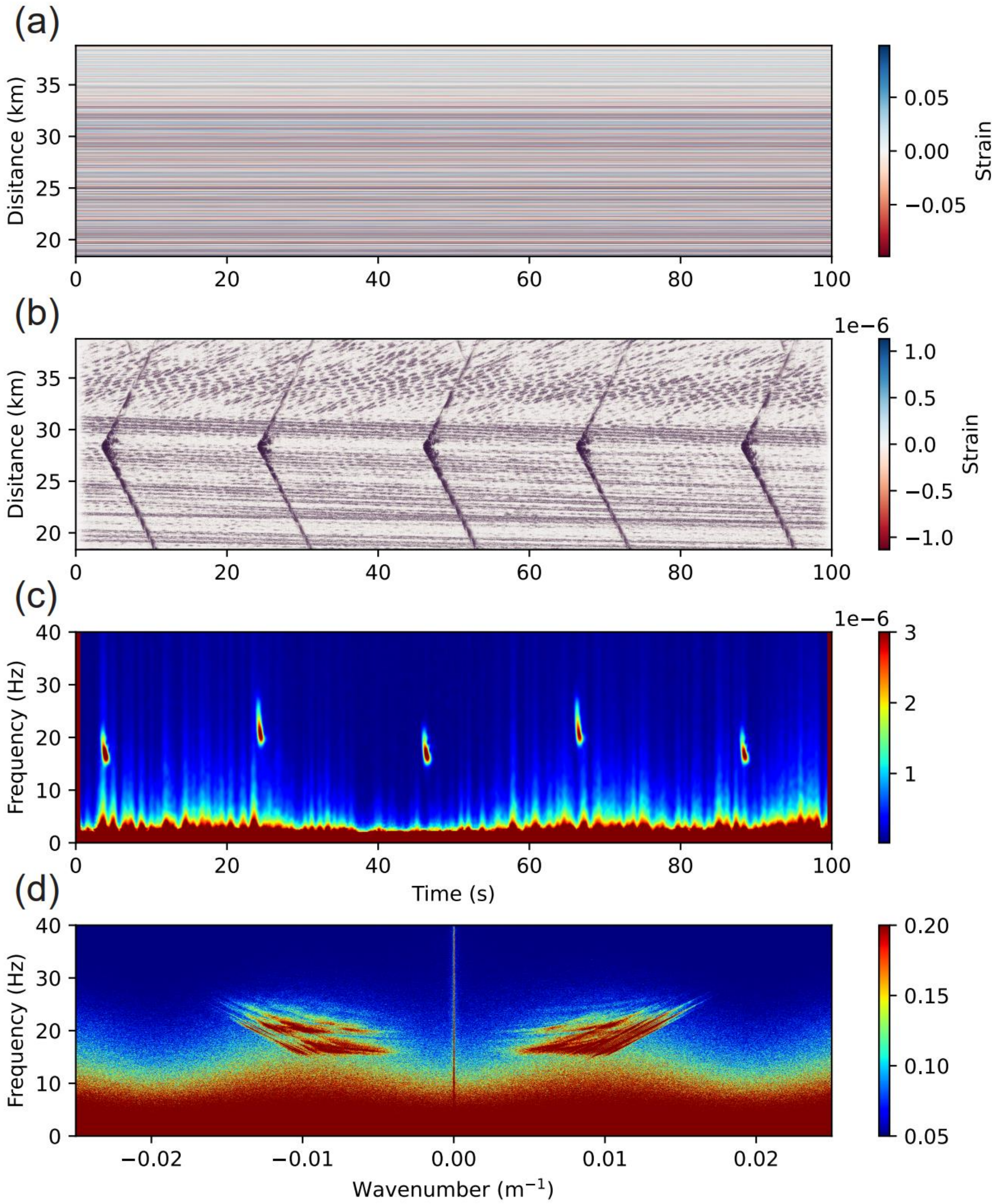

Figure 3. Demonstration of signal processing and visualization. (a) Original strain recording for 100 seconds beginning on November 4, 2021, 01:59:02 UT, recorded by the Optasense interrogator channel 9000-19000 on north ocean-bottom cable from RAPID dataset (Wilcock & Ocean Observatories Initiative., 2023). (b) Filter to 15-27 Hz, following Wilcock et al. (2023). (c) Spectrogram averaged over 100 channels. (d) FK spectrum calculated from 2D fast Fourier transform.

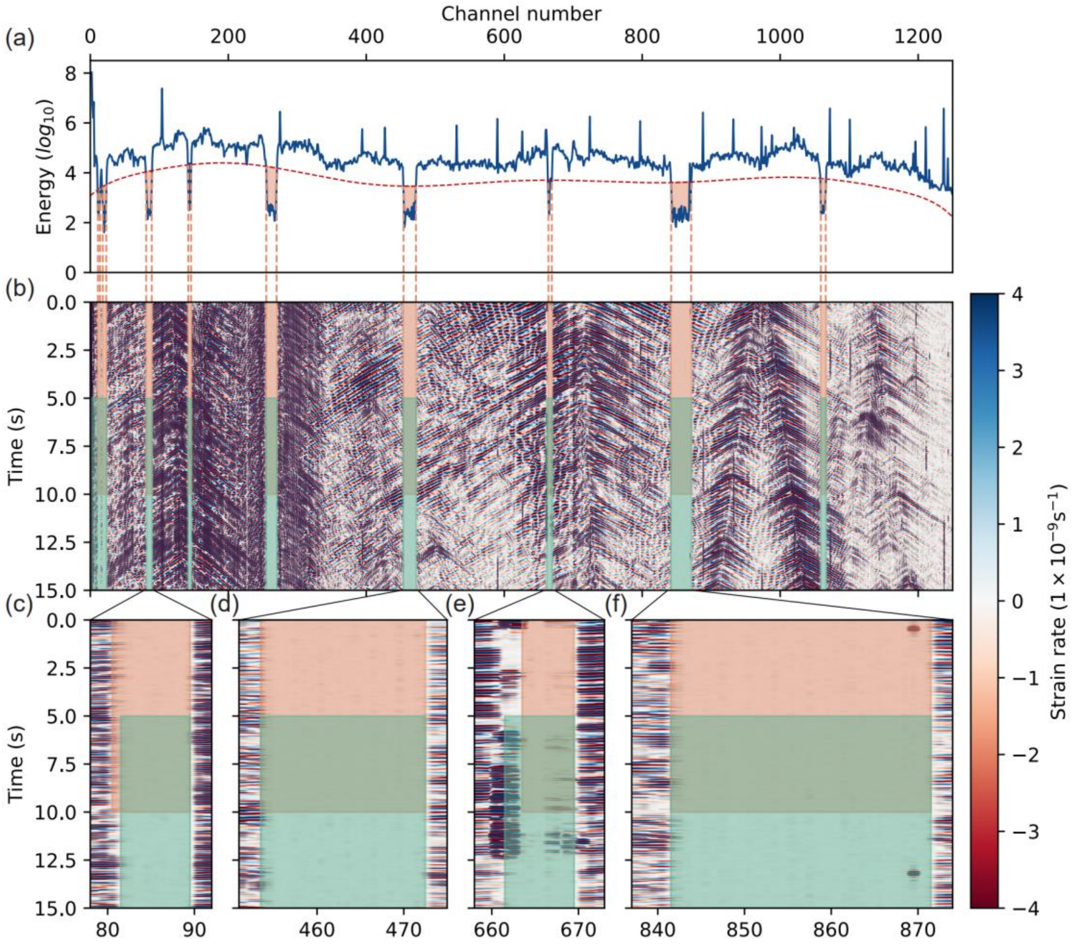

Figure 4. Bad channel detection of the DAS array near Ridgecrest, CA. (a) Energy curve (blue line) and thresholds (red dotted line) for bad channel detection. (b) DAS recording of 15-second traffic noise (Atterholt, 2021) used for bad channel detection. Orange areas indicate bad channels detected by our function, while green areas are bad channels picked by Atterholt, Zhan, Shen, et al. (2022). (c)-(f) Zoom-in plot of four parts of the DAS recording. Channel 81 (c) and channels 662&663 (e) are identified differently by our function and Atterholt, Zhan, Shen, et al. (2022).

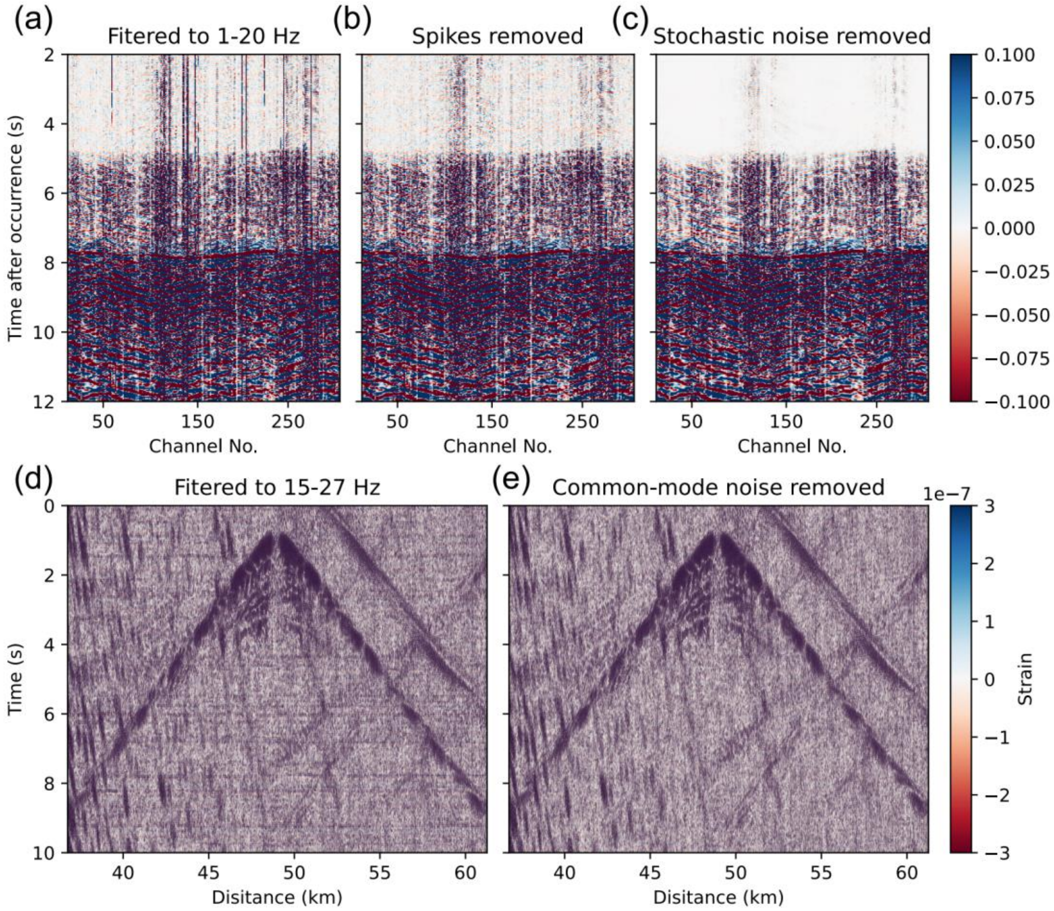

Figure 5. Cases of wavefield denoising. (a) Waveforms of an M_D 2.8 earthquake (https://earthquake.usgs.gov/earthquakes/eventpage/nc73940346/executive) recorded by Stanford-1 DAS array (Biondi et al., 2017; Martin et al., 2017). Bad channels are removed and bandpass filter to 1-20 Hz. (b) Waveforms with spikes removed based on (a). (c) Waveforms with stochastic noise removed by curvelet transform based on (b). (d) Strain recording filtered to 15 to 27 Hz for 10 seconds beginning on November 4, 2021, 01:59:22 UT, recorded by the Optasense interrogator on north ocean-bottom cable from RAPID dataset (Wilcock & Ocean Observatories Initiative., 2023). (e) Waveforms with common-mode noise removed based on (d).

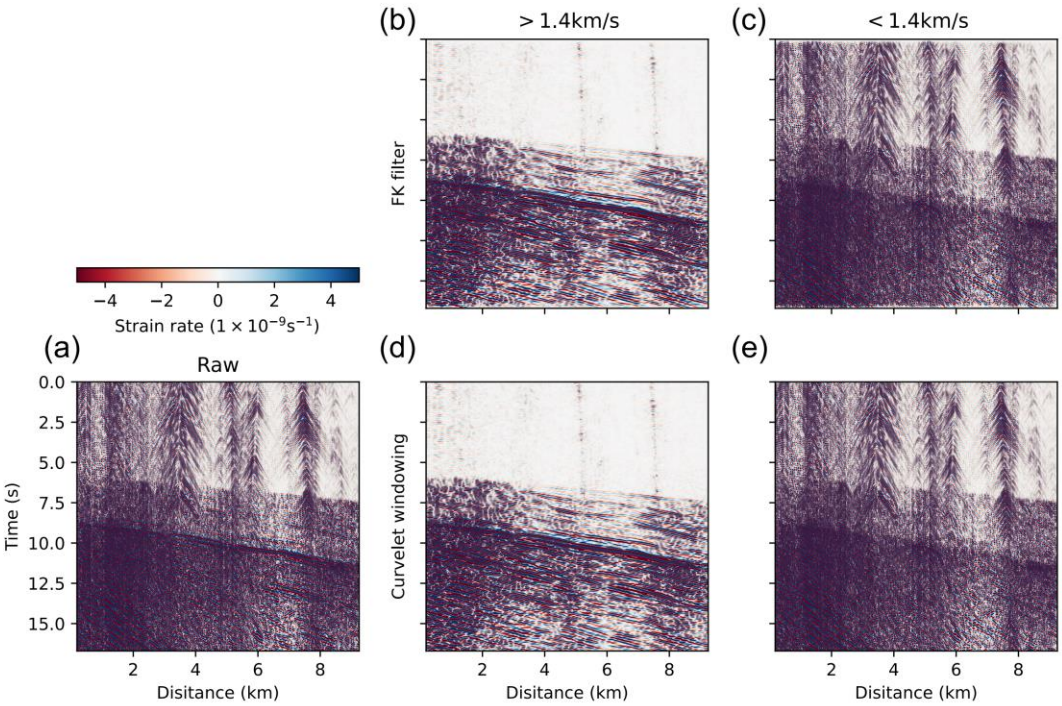

Figure 6. An example of wavefield decomposition. (a) Waveforms of an M_L 2.6 earthquake (https://earthquake.usgs.gov/earthquakes/eventpage/ci38972328/executive) recorded by Ridgecrest DAS array (Z. Li et al., 2021), with spikes removed. (b) Waveforms with an FK filter to retain energy with an apparent velocity >1.4 km/s (cosine tapered from 1.2–1.6 km/s). (c) Waveforms with an FK filter to retain energy with an apparent velocity <1.4 km/s (cosine tapered from 1.2–1.6 km/s). (d) Waveforms with curvelet windowing to retain energy with an apparent velocity >1.4 km/s. (e) Waveforms with curvelet windowing to retain energy with an apparent velocity <1.4 km/s.

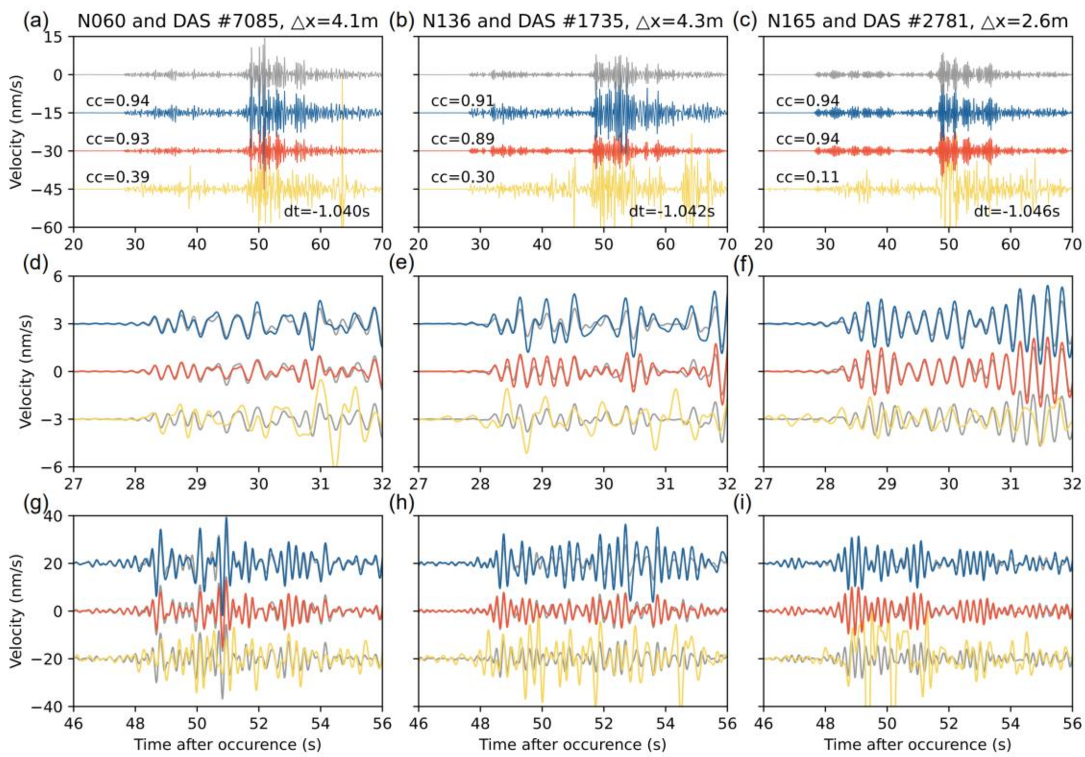

Figure 7. Conversion from strain to velocity by three methods of M_L 4.3 Hawthorne earthquake (https://earthquake.usgs.gov/earthquakes/eventpage/nn00536374) recorded by Brady's geothermal field DAS array. (a)-(c) Rotated geophone velocity (grey), and velocity converted from integrated DAS strain by FK-rescaling (blue), curvelet transform (red) and time-domain slowness determination (yellow), same as below. All waveforms are bandpass filtered to 1-5 Hz. (d)-(f) Zoom-in window for P arrival of (a)-(c). (g)-(i) Zoom-in window for S arrival of (a)-(c).